

Analysis of Vibration Characteristics of Vehicle-Track Vertically Coupling System Excited by Harmonic Waves based on Improved EMD

Hua Jiang^{1,2}, Jianhui Lin²

¹School of Information Science and Technology, Southwest Jiaotong University
Chengdu, 610031, China.

²Traction Power State Key Laboratory, Southwest Jiaotong University
Chengdu, 610031, China.
jhtgzyyx@163.com

Received February, 2018; revised May, 2018

ABSTRACT. *The model of vehicle-track vertically coupling system is built based on the theory of vehicle-track coupling dynamics. The vibration characteristics of vehicle-track vertically coupling system excited by harmonic waves are analyzed. A generalized intrinsic mode function is defined, and the improved EMD is used to extract vibration characteristics of vehicle-track vertically coupling system excited by harmonic wave. The result shows: the amplitude of wheel set acceleration raises in power function with the increase of vehicle velocity in liner range. The oscillation period of wheel set is related only to the period of harmonic wave. Using the same end condition, the wheel set acceleration can be decomposed preferably, each harmonic responses can be extracted by improved EMD, the end point effect decreases significantly.*

Keywords: A generalized intrinsic mode function; Vehicle-track vertically coupling system; Harmonic excitation

1. Introduction. Track irregularity is random, usually can be described by single or multiple harmonic approximately. For example, the vertical irregularity of railhead squats, switch areas (point rail) is the single harmonic excitation. The vertical irregularity of rail corrugation is continuous harmonic excitation. When wheels centroid deviates geometric center, the vertical irregularity is periodic harmonic wave excitation. Due to the interaction of vehicle and track, the irregularity would increase gradually, also it is easy to cause vehicle parts loosening and fatigue damage.

In the research on detection technology of track, the most common method is non-contact ultrasonic technique. Although, ultrasonic testing has been used to diagnose track defect, but these methods are only used for crack detection. In the basis of the ultrasonic flaw detector, a new technology of high speed testing has been developed. A new low frequency eddy current rail car has been developed, the detection rate is up to 80km/h in the United States. But eddy current testing can only detect defects which are on the surface or near surface layer.

With the development and popularization of computer, the improvement of computer image processing and simulation technology has been developed rapidly^[1-8]. In recent years, some foreign research institutions are engaged in this area, and put forward some effective methods. In Austria, Deutschl^[3] used two different color line scan camera, got the image with the method called a spectral image difference, the rail surface damage can

be detected automatically. This method is simple but need image acquisition equipment with special requirements. In Italy, Nitti et al.^[4] used gradient method, detected the track surface by investigating the changes of pixel gray value of rail surface image, and used neural network classifier to realize classification of injury automatically. Because this method need calculate the gradient, so the algorithm is complex and time-consuming. Through the analysis of rail surface texture features, Mandriota^[5] proposed the detection method of rail surface corrugation. Cesare Alippi^[6] proposed a comprehensive method using image processing to exact orbit contour. High speed detection can be realized through pre filter algorithm to limit the image region containing track contour, neural remodeling can achieve high precision orbit contour detection. In [7], the author used the Fourier transform profilometry, a three-dimensional and non-contact optical measurement method, for recovering the rail profile and defects on the rail web. P.V.V. Kishore^[8] used computer vision to find defective bogie parts with the moving train around 30Kmph. However, the machine vision method can only detect surface defects.

Another way to detect or predict the rail defects is the axle box acceleration (ABA). Because of the action of wheel-rail, the ABA can be used for measuring the vibration of vehicle-track system. It can be used for the identification of the track irregularity in the wheel-rail interface. Grassie^[9] thought that ABA measurement technology is superior to other rail longitudinal profile measurement technology, is capable of on-line measurement of track irregularity. In addition, ABA measurement technology has many other advantages. First of all, the crack detection is not inevitable, furthermore, non crack defects can also be measured. This method can also obtain the dynamic contact force. In addition, because the accelerometer can be easily installed in the many standard vehicles which are running, so the ABA measurement does not need complex instrument. Therefore, automatic detection of short track defects and the non intrusive monitoring of railway network can be realized by ABA. Sunaga et al. ^[10–13] used finite element modeling to analyze the influence on axle box acceleration excited by different defects, such as squat, weld joint with bad welding quality, rail insulation joint and corrugation. Wheel flat and corrugation can cause periodic dynamic interaction between wheel and rail, and generate vibration at a specific frequency. Marija molodova, Z. Li et al. ^[13–20] use this method to detect the larger black spots successfully, while the detection rate of small squats is 67%. But there is a contradiction between the acceleration signals of the axle box of the weld joints.

Although these scholars used the finite element modeling to analysis of the effect of ABA excited by surface defects, but did not consider the suspension system of vehicle track system.

In order to explore the time-frequency characteristics of vehicle, track, and bridge coupling system, Chen shuangxi et al.^[21–24] established models of vehicle-track and vehicle-track-bridge coupling system. Chen adopted improved extremum field mean mode decomposition method to improve the accuracy of the local mean. Wheel-rail force, acceleration of bogie and car body were decomposed by the Improved EMD when corrugation and the track irregularity excite the vehicle synchronously. He thinks that the main components of wheel-rail force are caused by corrugation and the low and medium frequency component amplitudes of bogie acceleration are greater than the high frequency component. However, the decomposition results are given in terms of time-frequency vs wheel-rail force, time-frequency vs accelerations etc, and cant consistent with the actual defects in space. Subsequently, Chen explored the time-frequency characteristics of vehicle-track and vehicle-track-bridge coupling system with wheel tread defect. Using improved EMD, the vertical vibration of car body is decomposed. The time-frequency spectrum and Hilbert marginal spectrum clearly describe the nonlinear variation of the frequency and

amplitude of car body vibration component. The vibration caused by defects increases with the increase of cars speed, the vibration belongs to the high frequency vibration. However due to the vehicle suspension system, the high frequency vibration of wheel are filtered.

In recent years, many scholars^[25–28] have devoted themselves to the analysis of ABA by signal analysis to extract the characteristics of track irregularities.

Weng Liangfeng^[25] adopted the harmonic wavelet to extract low frequency of track irregularity signal under strong interference. In order to guarantee the reliability of the result, the Daubechies, the Meyer and the Harmonic wavelet families are employed to make a compare. The result indicated that the Daub9, the Meyer and the harmonic wavelet can eliminate strong interference in the signal, and extract the characteristic frequency. However, only the harmonic wavelet can extract the weak periodic signals successfully.

Hsin-chu Tsai etc.^[26] adopted Hilbert-Huang transform (HHT) technique to analysis axle-box acceleration. The method can effectively identify and detect specific irregularity wavelength components, and the results are matching with the data measured by track inspection car. Furthermore, this paper also proposed a restoration method of real track irregularity geometry by using 10-m-chord versine data from track inspection car for obtaining the complete track irregularity waveform. Hsin-Chu Tsai etc.^[27] applies an inspection technique previously reported in the literature to on-site testing of track. The response to vibrations on railway bridges, track system components and track irregularities are also studied. The data is decomposed by EEMD, the frequency span can be obtained using its marginal spectrum. Caution must be exercised, however, as on-site test results show that the signal response measured by a moving vehicle cannot easily and clearly identify bridge vibration responses and frequencies unless a sophisticated analysis method is used.

Deng Xiaojun^[28] adopts ensemble empirical mode decomposition (EEMD) Hilbert transform and orthogonal NHT to analyze the vertical wheel-rail force and bogie vertical acceleration excited by long wave corrugation which has different wavelength and wave depth. He thought that corrugation will cause frequency modulation of the vibration response of vehicle system.

The vibration of vehicle-track vertical coupling system has the characteristics of non-linear and non-stationary. Traditional Fourier transform is not suitable for the analysis of non-stationary vibration signal. To reflect the local characteristics of signal, the short-time Fourier transform can solve the problem, but the difference of window function can conduct a greater impact on the results of the analysis. Wavelet transform can fully highlight the characteristics of some aspect of the problem, can focus on localization analysis of time/space frequency, can automatically adapt to the requirements of time-frequency signal analysis, which can focus on any details of signal. But wavelet transform must predefine basis function and isnt adaptive. At the same time, all of above transformation methods comply with the uncertainty principle.

Huang et al^[30] proposed empirical mode decomposition (EMD) which is a new method to analyze non-stationary, nonlinear non-Gaussian signal adaptively. An improved EMD method is used to analyze the time-frequency characteristics of vehicle-track coupling systems vibration with harmonic excitation in the article.

2. Vehicle- track coupling dynamic model. The vehicle-track vertical system model is the foundation of the vehicle-track vertical coupling system dynamics. The model of vehicle-track vertical system regards the vehicle system and rail system as an interacting and coupling system. The wheel-rail vertical forces are confirmed by Hertz nonlinear

elastic contact theory. The wheel set dynamic responses which are excited by different harmonic waves in different velocity are studied.

Considering monorail vertical excitation, the model of vehicle-track vertical system adopts parameters of high speed model car (HSC). These parameters are summarized in Table 1.

TABLE 1. Table1 vehicletrack simulation parameters^[29]

| Parameters, Notation(unit) | Value | Parameters, Notation(unit) | Value |
|--|--------------------|---|--------------------|
| Carbody mass, $M_c(Kg)$ | 52000 | Rail pad stiffness, $K_p(N/m)$ | 6×10^7 |
| Bogie mass, $M_t(Kg)$ | 3200 | Rail pad damping, $C_p(N \cdot s/m)$ | 7.5×10^4 |
| Wheelset mass, $M_w(Kg)$ | 1400 | Ballast stiffness, $K_b(N/m)$ | 2.4×10^8 |
| Carbody mass inertia, $J_c(Kg \cdot m^2)$ | 2.31×10^6 | Ballast damping, $C_b(N \cdot s/m)$ | 6×10^4 |
| Bogie mass inertia, $J_t(Kg \cdot m^2)$ | 3120 | Subgrade stiffness, $K_f(N/m)$ | 6.5×10^7 |
| Primary suspension stiffness of vehicle, $K_{pz}(N/m)$ | 1.87×10^6 | Subgrade damping, $C_f(N \cdot s/m)$ | 1×10^5 |
| Primary suspension damping of vehicle, $C_{pz}(N \cdot s/m)$ | 5×10^5 | Ballast shear stiffness, $K_w(N/m)$ | 7.84×10^7 |
| Secondary suspension stiffness of vehicle, $K_{sz}(N/m)$ | 1.72×10^6 | Ballast shear damping, $C_w(N \cdot s/m)$ | 8×10^4 |
| Secondary suspension damping of vehicle, $C_{sz}(N \cdot s/m)$ | 1.95×10^5 | Ballast pressure diffusion angle, $\alpha(^{\circ})$ | 35 |
| half of bogies distance, $l_c(m)$ | 9 | Ballast elastic modulus, $E_b(Mpa)$ | 1.2×10^8 |
| half of wheelsets distance, $l_t(m)$ | 1.25 | Ballast thickness, $h_b(m)$ | 0.35 |
| Wheel radius, $R(m)$ | 0.4575 | Effective supporting length of half sleeper, $l_e(m)$ | 1.175 |
| Rail mass per unit length, $M_p(Kg/m)$ | 60.64 | Average width of sleeper bottom, $l_b(m)$ | 0.277 |
| Rail bending stiffness, $EI(N/m^2)$ | 6.62×10^6 | Sleeper spacing, $l_s(m)$ | 0.6 |
| Sleeper mass, $M_s(Kg)$ | 340 | Subgrade K_{30} modulus, $E_f(Mpa/m)$ | 1.9×10^8 |
| | | Ballast density, $\rho_b(Kg/m^3)$ | 1.9×10^3 |

A half vehicle vertical system model which consists of car body, bogie, primary suspensions, second suspensions and wheels is established as shown in Figure 1^[29]. The vehicle system is regarded as a multi-rigid body system with a speed of V , has ten degrees of freedom such as the ups and downs of car body Z_c , nod of car body β_c , the ups and downs of front and rear frames $Z_{ti}(i=1,2)$, nods of front and rear frames $\beta_{ti}(i=1,2)$ and vertical vibration of four wheel sets $Z_{wi}(i=1-4)$.

For the track part, spring-damping vibration model which includes three layers (rail-sleeper-ballast-subgrade) is established. The rail is regarded as continuous infinite Euler beam which is supported by elastic discrete points, the foundation under rail is separated along the longitudinal direction, each sleeper fulcrum is a discrete unit, each supporting unit adopts double mass (sleeper quality M_{si} and ballast quality M_{bi}).

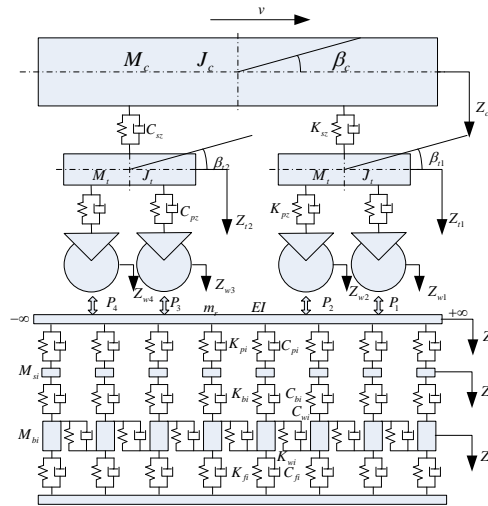


FIGURE 1. vehicle-track vertical coupling system model

By using Hertz nonlinear elastic contact theory, the vertical coupling relationship between vehicle and track is established, i.e.

$$p_j(t) = \begin{cases} \frac{1}{G} [Z_{wj}(t) - Z_r(x_{wj}, t) - Z_0(t)]^{3/2} & \text{wheel-rail contact} \\ 0 & \text{wheel-rail departure} \end{cases} \quad (1)$$

The dynamic equations of vehicle-track coupling system are unified into $[M]\{\ddot{X}\} + [C]\{\dot{X}\} + [K]\{X\} = \{P\}$. $[M], [C], [K]$ are the mass, damping and stiffness matrices of the vehicle-track coupling system respectively. $\{X\}$ is the generalized displacement vector, $\{\dot{X}\}$ is the generalized velocity vector, $\{\ddot{X}\}$ is the generalized acceleration vector, $\{P\}$ is a generalized load vector.

3. Improved EMD(IEMD). After a thorough study of the concept of instantaneous frequency, HHT is an founded by American Chinese, Norden, e., Huang, et al. The concept of intrinsic mode functions and the method of decomposing arbitrary signals into intrinsic modal functions are proposed in Empirical Mode Decomposition (EMD) method, reasonable definitions of instantaneous frequency, physical meaning and solution are also given in this method.

The necessary conditions for defining a meaningful instantaneous frequency in physics are that the function is symmetric relative to the local zero mean and the number of zero crossing points equal the number of extrema. Therefore, Huang proposes a function that satisfies the following two conditions, i.e.^[30,31]

- (1) In the whole data set, the number of extrema and the number of zero crossings must either equal or differ at most by one;
- (2) At any point, the mean value of the envelope defined by the local maxima and the envelope defined by the local minima is zero.

In the definition of the intrinsic mode function of Huang, any IMF is a continuous narrowband signal, and is the continuous intrinsic mode of this frequency. In practical engineering, there are a large number of signals, and one of their intrinsic modes is not necessarily continuous, modal aliasing will appear in the decomposition of this signals. Therefore, a generalized intrinsic mode function is proposed:

(1) In a whole data set, a signal consists of one or more segments satisfying a characteristic scale. For each segment, the number of extrema and the number of zero crossings must either equal or differ at most by one;

(2) At any point, the mean value of the envelope defined by the local maxima and the envelope defined by the local minima is zero.

The generalized intrinsic mode function is composed of several sectionalized intrinsic modal functions, and each segment of generalized intrinsic modal functions is the same narrow band signals, which are the sectionalized intrinsic mode functions of this frequency with different length of time.

The steps to decompose a signal into several IMF's using the improved EMD method are described as follows:

(1) Firstly, the local maxima and minima of $x(t)$ are identified separately. Once the extrema are identified, all the local maxima are connected by a cubic spline line as the upper envelope $u(t)$. Repeat the procedure for the local minima to produce the lower envelope $v(t)$. The upper $u(t)$ and lower envelopes $v(t)$ should cover all the data between them. Their mean is designated as $m(t)=[u(t)+v(t)]/2$.

(2) The difference between the data and $m(t)$ is the first component, $h_1(t)$, i.e. $h_1(t)=x(t)-m(t)$ and then we determine whether $h_1(t)$ satisfies the generalized IMF requirement, if the generalized IMF condition is not satisfied, then $x(t)$ is replaced by $h_1(t)$. The upper and lower envelope $u_1(t)$ and $v_1(t)$ of $h_1(t)$ are obtained, and the above process is repeated, the upper and lower envelope mean $m_1(t)$ is obtained,

$$\begin{aligned}
 m_1(t) &= [u_1(t) + v_1(t)]/2 \\
 h_2(t) &= h_1(t) - m_1(t) \\
 \dots & \\
 m_{k-1}(t) &= [u_{k-1}(t) + v_{k-1}(t)]/2 \\
 h_k(t) &= h_{k-1}(t) - m_{k-1}(t)
 \end{aligned}
 \tag{2}$$

until the $h_k(t)$ obtained through above method satisfies the generalized IMF condition. Hence, the first generalized IMF is $C_1(t)=h_k(t)$

$$r_1(t) = x(t) - C_1(t). \tag{3}$$

(3) the steps(1)-(2) are repeated to the rest of the signal $r_1(t)$. Decomposition continues, until the remaining portion is a monotonic signal or whose value is less than a given threshold, and then the decomposition is over.

(4) All IMF components and residue are eventually obtained:

$$r_2(t) = r_1(t) - C_2(t), \dots, r_n(t) = r_{n-1}(t) - C_n(t) \tag{4}$$

(5) By summing up equations (3) and (4), we finally obtain the original signal $x(t) = \sum_{i=1}^n C_i(t) + r_n(t)$

4. Characteristic analysis of coupled system under harmonic excitation. Rail profile can be described by cosine function, when the vehicle is excited by single harmonic signal, i.e.

$$z_0(t) = a(1 - \cos \omega t)/2 \quad 0 \leq t \leq L/v \tag{5}$$

with, $\omega = 2\pi v/L$, L is wavelength of irregularity, a is wave depth of irregularity^[29].

The track harmonic irregularity is applied to the vehicle-track vertical coupling system model. The degree of freedom of the system is more and the system is complex nonlinear,

so the new explicit integration method proposed by Zhai Wanming is used to solve the problem.

4.1. Single harmonic excitation. When the wavelength of track irregularity is 10m and the wave depth is 5mm, the vertical accelerations of the wheel set are shown in Figure 2, the oscillation periods of acceleration are consistent with the long wave irregularity periods. The maximum accelerations of wheelset are $9.4209m/s^2, 6.8719m/s^2, 4.7692m/s^2, 3.0499m/s^2, 1.7146m/s^2$ respectively, when the velocities of the vehicle are 350km/h, 300km/h, 250km/h, 200km/h, 150km/h. With the increase of speed, the accelerations of wheelset are increased by power function(the fitting outcome is $(v_{max} = 5.771 \times 10^{-5} \times V^{2.048} + 0.07163)$). When the velocity of car is 350km/h, the acceleration of wheelset has nonlinear distortion near the maximum.

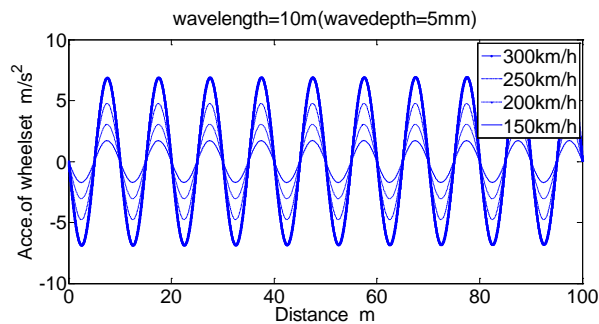


FIGURE 2. vertical acceleration of wheelset when a single harmonic excites (wavelength is 10m, wave depth is 5mm)

When the coupling system is excited by single harmonic signal with 10m wavelength and 5mm wave depth, the decomposition results of the vertical acceleration using IEMD, EMD, EEMD respectively are shown in Fig.3, Fig.4 and Fig.5.

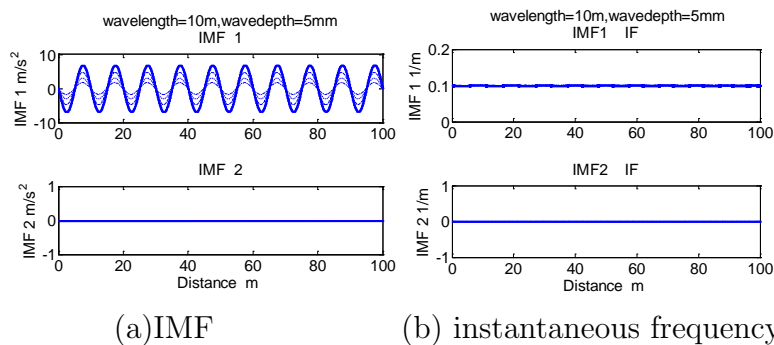


FIGURE 3. decomposition results of wheelset vertical acceleration excited by a single harmonic signal with using IEMD

Using IEMD, the extreme values of IMF1 are basically identical, are $6.87m/s^2, 4.77 m/s^2, 3.05 m/s^2, 1.71 m/s^2$ respectively, when the car speeds are 300km/h, 250km/h, 200km/h, 150 km/h. The decomposition results are almost no end effects. The space frequencies of the IMF1 are $0.1m^{-1}$, which are corresponding to the wavelengths of track irregularity. The decomposition results are good, and coincide with the actual situation.

In the same end condition, the maximum extreme value are $8.37m/s^2, 5.81m/s^2, 3.71m/s^2, 2.09m/s^2$, when the distances are 7.41m, 7.38m, 7.34m, 7.38m, the minimum

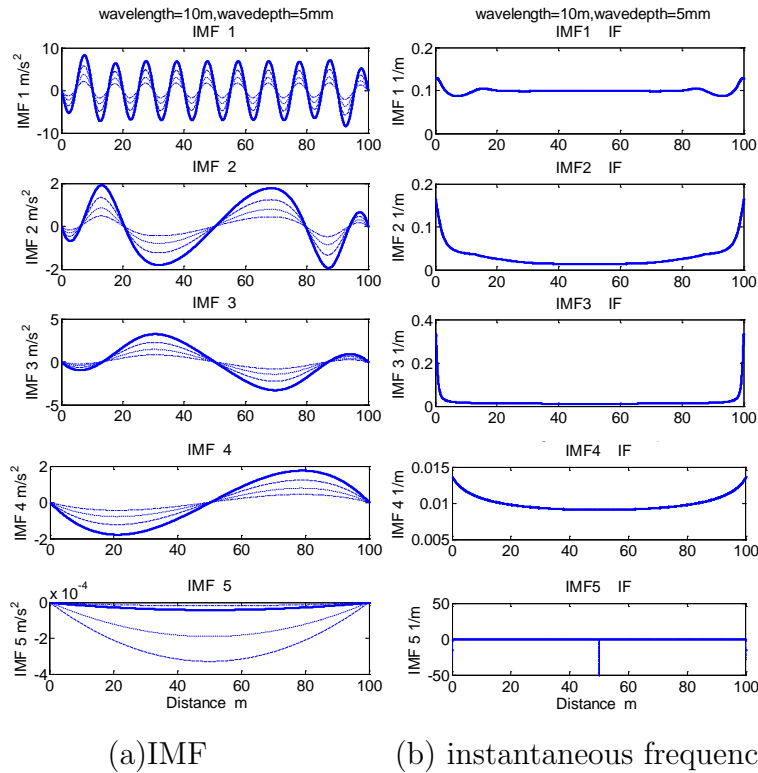


FIGURE 4. decomposition results of wheelset vertical acceleration excited by a single harmonic signal using EMD

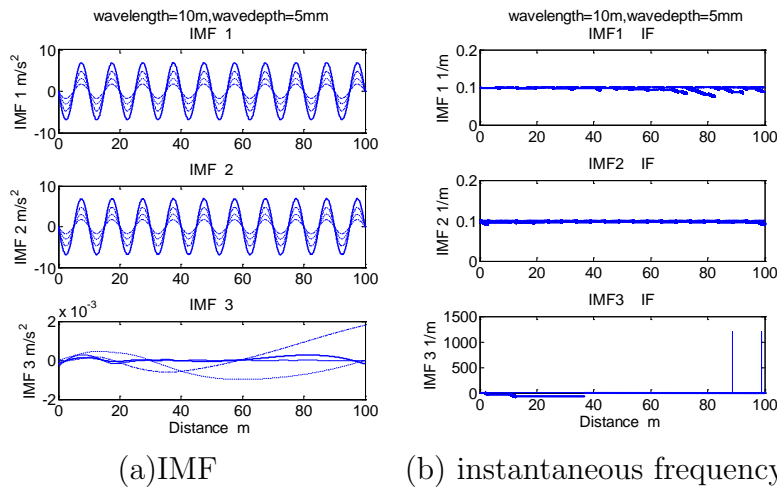


FIGURE 5. decomposition results of wheelset vertical acceleration excited by a single harmonic signal using EEMD

of extreme value are $-8.37m/s^2$, $-5.81m/s^2$, $-3.67m/s^2$, $-2.08m/s^2$, when the distances are 92.62m,92.62m,92.78m, 92.78m(with the car speeds are 300km/h,250km/h,200km/h,150 km/h respectively). The ratios of the first maximum to the second maximum are 129.21%, 129.36%, 129.04%, 129.33%, the ratios of the first minimum to the second minimum are 129.21%, 129.25%, 127.65%, 128.71%. Obviously, the results obtained from EMD have significant endpoint effects. The instantaneous space frequency of first IMF using EMD fluctuates around $0.1m^{-1}$, coincide with the actual situation nearly. But the

maximum of instantaneous spatial frequency is 0.1296, when the car speed is 300km/h, the frequency obtained from EMD is above theoretical frequency 29.6%. Because of the significant endpoint effect, the multiple IMF components appear, and result in energy dispersion.

Using EEMD, two identical IMFs are obtained. The extreme values of IMF1 and IMF2 are basically identical, are $6.87m/s^2$, $4.77m/s^2$, $3.05m/s^2$, $1.71m/s^2$ respectively, when the car speeds are 300km/h, 250km/h, 200km/h, 150km/h. The decomposition results are almost no end effects. The space frequencies of the IMF1 and IMF2 both are $0.1m^{-1}$ and coincident, redundant decomposition results are obtained. The energy percentages of the two IMFs are 50.001%, 49.999% respectively. Due to the limited space, only the first three IMF decomposition results are given (In order to compare the decomposition effect of IEMD, the noise group number is one, and the noise variance is zero).

The energy percentage of decomposition results using three methods at different velocities are shown in Table 2.

TABLE 2. energy percentage of decomposition results using three methods at different velocities when a single harmonic excites

(wavelength is 10m, wave depth is 5mm)

| % | IMF1 | IMF2 | IMF3 | IMF4 | IMF5 |
|-------------------------------|--------|--------|--------|-------|------|
| IEMD(300 /250/200 /150) | 100 | 0 | - | - | - |
| | 100 | 0 | - | - | - |
| | 100 | 0 | - | - | - |
| | 100 | 0 | - | - | - |
| EMD(300 /250/200 /150) | 77.447 | 4.887 | 12.446 | 5.220 | 0 |
| | 77.448 | 4.886 | 12.446 | 5.220 | 0 |
| | 77.452 | 4.886 | 12.444 | 5.218 | 0 |
| | 77.455 | 4.887 | 12.441 | 5.216 | 0 |
| EMD(300 /250/200 /150) | 50.001 | 49.999 | 0 | 0 | 0 |
| | 50.001 | 49.999 | 0 | 0 | 0 |
| | 50.001 | 49.999 | 0 | 0 | 0 |
| | 50.001 | 49.999 | 0 | 0 | 0 |

4.2. Bi-harmonic excitation. When the track is simultaneously excited by two harmonic irregularities (When the wavelength is 10m, the wave depth is 5mm, and when the wavelength is 5m, the wave depth is 1mm), the vertical accelerations of the wheel set are shown in Figure 6. The oscillation periods of acceleration are consistent with the two long wave irregularity periods. The maximum accelerations of wheel set are $17.0286m/s^2$, $12.4192m/s^2$, $8.6082m/s^2$, $5.4995m/s^2$, $3.0892m/s^2$ respectively, when the velocities of the vehicle are 350km/h, 300km/h, 250km/h, 200km/h, 150km/h. With the increase of speed, the accelerations of wheel set are increased by power function (the fitting outcome is $(v_{max} = 1.025 \times 10^{-4} \times V^{2.051} + 0.1248)$). When the velocity of car is 350km/h, the acceleration of wheel set has also nonlinear distortion near the maximum.

When the coupling system is excited by bi-harmonic signal with 10m wavelength, 5mm wave depth and 5m wavelength, 1mm wave depth, the decomposition results of the vertical acceleration using IEMD, EMD, EEMD respectively are shown in Fig.7, Fig.8 and Fig.9.

When the IEMD decomposition is used, the end effect is not significant. The higher frequency component IMF1 is mixed with partial signals of low frequency components.

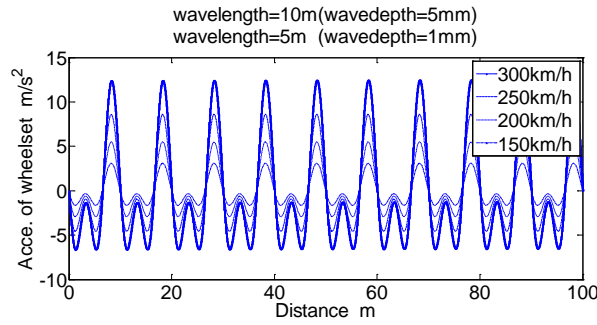


FIGURE 6. vertical acceleration of wheelset when bi-harmonic excites (wavelength is 10m,wave depth is 5mm wavelength is 5m,wave depth is 1mm)

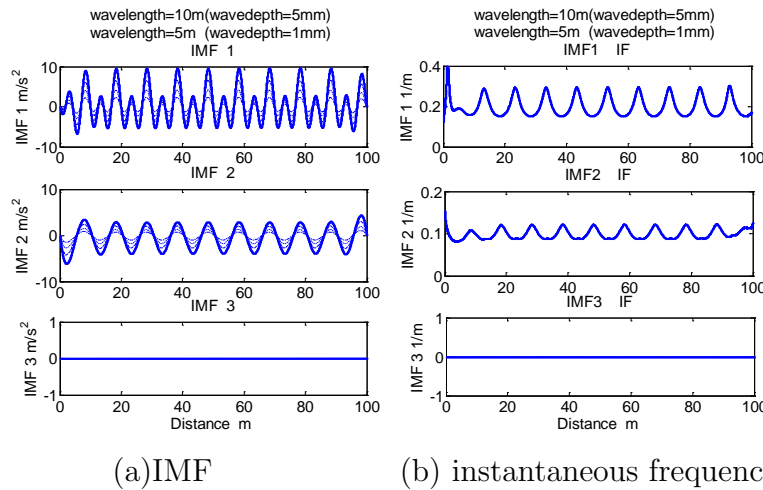


FIGURE 7. decomposition results of wheelset vertical acceleration excited by bi-harmonic signal using IEMD

Due to energy leakage, the amplitudes of even peaks increase in IMF1. The lower frequency component IMF2 is extracted accurately. The energy percentages of the two IMFs are 75%, 25% respectively. The spatial instantaneous frequency of IMF1 is wavy, the spatial frequency is fluctuated around 0.2m^{-1} , the spatial frequency is corresponding to the harmonic excitation having 5m wavelength. The maximum spatial frequency of IMF1 are $0.4448\text{ m}^{-1}, 0.4437\text{ m}^{-1}, 0.4423\text{ m}^{-1}, 0.4405\text{ m}^{-1}$, the average value of peaks are $0.2954\text{ m}^{-1}, 0.2952\text{ m}^{-1}, 0.2950\text{ m}^{-1}, 0.2947\text{ m}^{-1}$, corresponding to the speed 300km/h, 250km/h, 200km/h, 150km/h. The ratios of maximum and average value of peaks are 1.5058, 1.5030, 1.4493, 1.4947. The fluctuation of spatial frequency in IMF2 is weaker than IMF1s. The spatial frequency of IMF2 is fluctuated around 0.1m^{-1} , and the spatial frequency of IMF2 is corresponding to the harmonic excitation having 10m wavelength. The ratios of maximum and average value of peaks are 1.2573, 1.2573, 1.2583, 1.2593. The vehicle-track coupling relationship adopts the Hertz nonlinear elastic contact theory, so the nonlinear of vehicle-track system leads to the quasi periodicity of the vertical acceleration of wheel set. The instantaneous frequency of each IMF component obtained by IEMD decomposition shows obvious undulatory property, and the decomposition results are good, and agree with the actual situation.

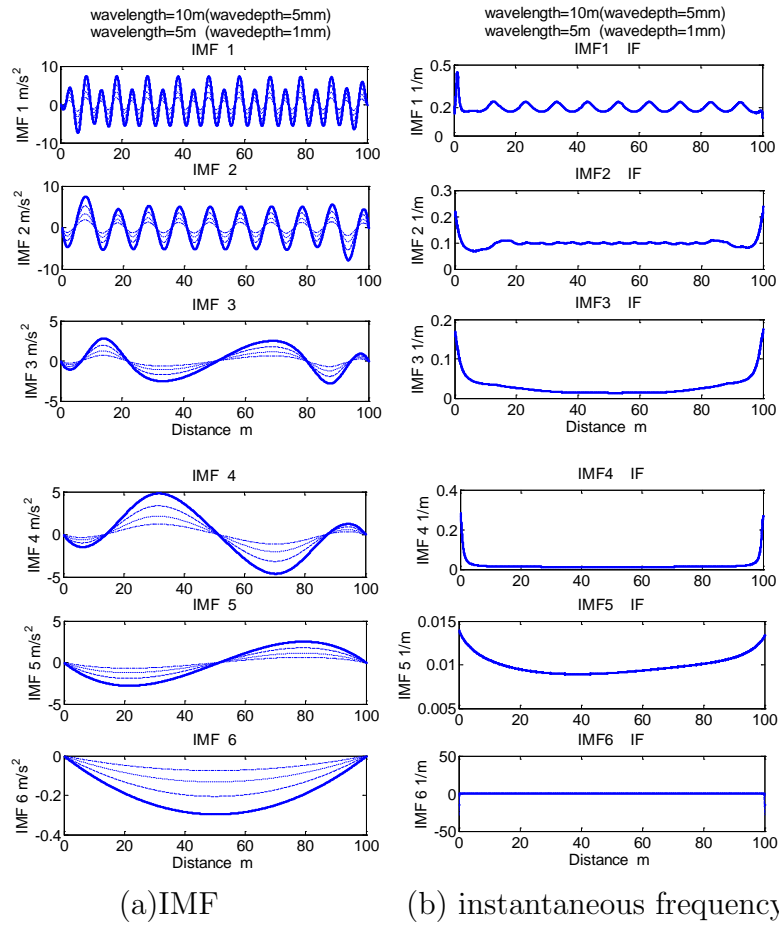


FIGURE 8. decomposition results of wheelset vertical acceleration excited by bi-harmonic signal using EMD

Under the same termination condition, more IMF components appear using EMD, the energy of each IMF is dispersive. The maximum spatial frequency of IMF1 are $0.4518\text{m}^{-1}, 0.4510\text{m}^{-1}, 0.4449\text{m}^{-1}, 0.4485\text{m}^{-1}$, the average value of peaks are $0.2410\text{m}^{-1}, 0.2409\text{m}^{-1}, 0.2409\text{m}^{-1}, 0.2408\text{m}^{-1}$, corresponding to the speed 300 km/h, 250 km/h, 200 km/h, 150 km/h. The ratios of maximum and average value of peaks are 1.8747, 1.8721, 1.8468, 1.8625 respectively. In the same way, the ratios of maximum and average value of peaks are 2.1219, 2.1219, 2.1239, 2.1239 in IMF2. The ratios increase 69%. Obviously, when using EMD, the endpoint effect is significantly greater than that of using IEMD. In addition, the total energy of IMF1 and IMF2 is 2/3, the rest energy is scattered to the other IMFs.

The IMF1 obtained by using EEMD decomposition is similar to the original signal, and the spatial instantaneous frequency is showing a bridge type, the maximum of spatial instantaneous frequency 0.15m^{-1} , and the negative instantaneous frequency is obtained. This situation isn't identical with the actual situation. The IMF2 and IMF3 components correspond to the harmonic excitation of two wavelengths respectively, and the waveforms are similar to that of IEMD and EMD, but the fluctuation amplitude is smaller. But the fluctuation of instantaneous frequency between two adjacent sampling points is larger, what leads to which instantaneous frequencies of each IMF component have two branches, the phenomenon is especially significant at the ends. Redundant decomposition results appear. The energy of IMF1 is up to 50%, the energy of higher frequency component is nearly 20%, the energy of lower one is nearly 30%. Due to the redundant decomposition

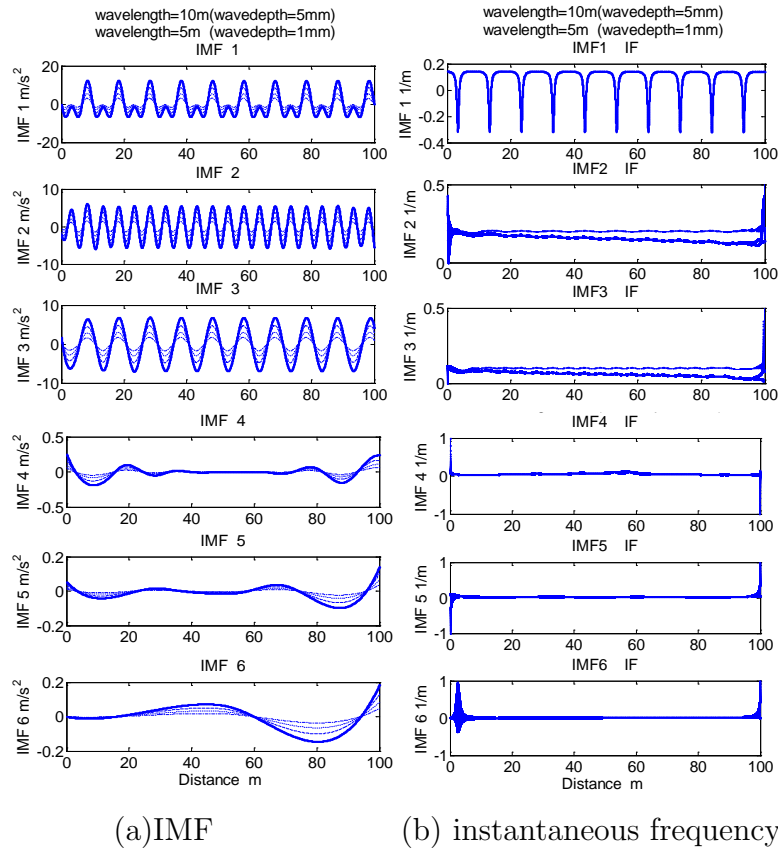


FIGURE 9. decomposition results of wheelset vertical acceleration excited by bi-harmonic signal using EEMD

results, the energy dispersion is more serious. In order to compare the decomposition effect of IEMD, the noise group number is one, and the noise variance is zero.

When the system is excited by two harmonic signals, the energy percentage of decomposition results using three methods at different velocities are shown in Table 3.

5. Conclusion. In this paper, a generalized intrinsic mode function is proposed for the classical EMD method. When an intrinsic mode is not continuous, i.e. the signal is comprised several sectional intrinsic modes which have same frequency, the method is effective and can avoid modal aliasing in the decomposition in a EMD decomposition. At the same time, the model of vehicle- track vertical coupling system is established. The accelerations of wheel set are calculated using this model, when the system is excited by single harmonic signal and bi-harmonic signals. When decomposing vertical acceleration excited by harmonic excitation can use the improved EMD method. Under the same criteria, the decomposition results are accurately, fewer components, the energy is concentrated and can effectively solve the problem of the endpoint using improved EMD.

Acknowledgment. This study was partly supported by Key Fund Project of Sichuan Provincial Education Department (NO.16ZA0153), Open Research Subject of Key Laboratory of Signal and Information Processing, Xihua University (NO.szjj2014-021). Chun-Hui Project of Ministry of Education of China (NO.Z2014077).

TABLE 3. energy percentage of decomposition results using three methods at different velocities when bi-harmonic excites

(wavelength is 10m,wave depth is 5mm
wavelength is 5m,wave depth is 1mm)

| % | IMF1 | IMF2 | IMF3 | IMF4 | IMF5 | IMF6 |
|-------------------------------|--------|--------|--------|--------|-------|-------|
| IEMD(300 /250/200 /150) | 75.192 | 24.808 | 0 | - | - | - |
| | 75.139 | 24.861 | 0 | - | - | - |
| | 75.093 | 24.907 | 0 | - | - | - |
| | 75.054 | 24.946 | 0 | - | - | - |
| EMD(300 /250/200 /150) | 36.585 | 31.645 | 6.599 | 17.217 | 7.854 | 0.100 |
| | 36.525 | 31.707 | 6.599 | 17.216 | 7.851 | 0.102 |
| | 36.476 | 31.763 | 6.597 | 17.211 | 7.850 | 0.102 |
| | 36.427 | 31.803 | 6.602 | 17.216 | 7.850 | 0.102 |
| EMD(300 /250/200 /150) | 50.768 | 19.607 | 29.572 | 0.009 | 0.002 | 0.040 |
| | 50.772 | 19.550 | 29.623 | 0.009 | 0.002 | 0.043 |
| | 50.775 | 19.504 | 29.668 | 0.009 | 0.002 | 0.041 |
| | 50.777 | 19.466 | 29.705 | 0.009 | 0.002 | 0.041 |

REFERENCES

- [1] P. Gullers, L. Andersson, R. Lunden, High-frequency wheel-rail contact forces-field measurements and influence of track irregularities, *Wear*, vol. 265, pp.1472–1478,2008.
- [2] Y. H. Liu , T. Liu, Q. L. Wang, S. W. Luo, Rail Surface Defects Detection Algorithm Based on Image Processing , *Computer Engineering*vol. 33, no. 11, pp.236–238,2007.
- [3] E. Deuil, C. Gasser, A. Niel, et al, Defect detection on Rail Surfaces By A Vision Based System,*Proc. of IEEE Intelligent Vehicles Symposium*, pp. 507–511, 2004.
- [4] M. Nitti, C. Mandriota, E. Stella, et al. Real Time Classification of Rail Defects,*Proc. of the 8th International Conference on Computer Aided Design, Manufacture and Operation in the Railway and Other Advanced Mass Transit Systems*, pp.335–344,2002.
- [5] C. Mandriota, M. Ntti, N.Ancona, et al. A Distance Filter-based Feature selection for Rail Defect Detection, *Machine Vision and Applications*, vol.15, no. 4, pp.179-185, 2004.
- [6] C. Alippi, E. Casagrande, F. Scotti, and V. Piuri, Composite Real-Time Image Processing for Railways Track Profile Measurement, *IEEE Transactions on instrumentation and measurement*, vol. 49, no. 3, pp.559-564, 2000.
- [7] S. X. He, J. L. Li, X. R. Gao, L. Luo, Application of FTP in flaw detection of rail web,*Optik - International Journal for Light and Electron Optics*, vol. 126, pp. 187–190, 2015.
- [8] P. V. V. Kishore, C. Raghava Prasad, Computer vision based train rolling stock examination, *Optik - International Journal for Light and Electron Optics*, vol. 132, pp.427–444, 2017.
- [9] S.L. Grassie. Measurement of railhead longitudinal profiles: a comparison of different techniques , *Wear*, vol. 191, pp. 245–251, 1996.
- [10] M. Moravcik, Response of Railway Track on Nonlinear Discrete Supports, *Vehicle System Dynamics Supplement* , vol. 24, pp.280–293, 1995.
- [11] Y. Sunaga, I. Sano, T. Ide. Practical use of axlebox acceleration to control the shortwave track irregularities,*Proceedings of the World Congress on Railway Research. Florence, Italy*, 1997.
- [12] M. Bocciolone, A. Caprioli, A. Cigada, A. Collina. A measurement system for quick rail inspection and effective track maintenance strateg, *Mechanical Systems and Signal Processing*, vol. 21, pp.1242–1254, 2007.
- [13] A. M. Remennikov, S. Kaewunruen, A review of loading conditions for railway track structures due to train and track vertical interaction, *Structural Control and Health Monitoring*, vol. 15, pp.207–234, 2008.
- [14] M. Molodova, Z. L. Li, R. Dollevoet, Axle box acceleration: Measurement and simulation for detection of short track defects, *Wear*, vol. 271, pp. 349–356, 2011.

- [15] Z. Li, X. Zhao, C. Esveld, R. Dollevoet, M. Molodova, An Investigation into the Causes of squat-correlation analysis and numerical modeling, *Wear*, vol. 265, pp.134–1355, 2008.
- [16] Z. Li, M. Molodova, R. Dollevoet, Detect ability of isolated short wave rail surface defects by way of axle box acceleration, *Proceedings of the 21st International Symposium on Dynamics of the Vehicles on Roads and Tracks (IAVSD2009), Stockholm, Sweden*, pp.17–21 August, 2009.
- [17] Z. Li, X. Zhao, M. Molodova, R. Dollevoet, The validation of some numerical predictions on squats growth, *in: Proceedings of the 8th International Conference on Contact Mechanics and Wear of Rail/Wheel Systems, Florence, Italy*, pp.15–18 September, 2009.
- [18] X. Zhao, Z. Li, R. Dollevoet, Solution of the wheel-rail rolling contact in elasticity and elastoplasticity using a transient finite element model, *Proceedings of the 8th International Conference on Contact Mechanics and Wear of Rail/Wheel Systems, Florence, Italy*, pp. 15–18, September, 2009.
- [19] Z. Li, X. Zhao, C. Esveld, R. Dollevoet. Rail stresses, strain and fatigue under dynamic wheel-rail interaction, *Proceedings of International Heavy Haul Conference Specialist Technical Session Kiruna, Sweden*, pp.11–13 June, 2007.
- [20] M. Molodova, Z. Li, R. Dollevoet, Numerical simulation of the axle box acceleration of a railway wheel rolling over a rail geometrical irregularity, *Proceedings of the 7th International Conference on Railway Bogies and Running Gears, Budapest, Hungary*, pp. 3–6 September, 2007.
- [21] S. X. Chen, J. H. Lin, J. Z. Chen, Dynamic characteristics extraction of vehicle-track vertically coupling system based on improved EMD, *Journal of vibration and shock*, vol.30, no. 8, pp.212–216, 2011.
- [22] S. X. Chen, J. H. Lin, J. Z. Chen, Time-frequency characteristics extraction for vehicle /bridge coupled system based on Hilbert-Huang transformation, *Journal of vibration and shock*, vol. 31, no. 15, pp. 175–179, 2012.
- [23] S. X. Chen, J. H. Lin, J. Z. Chen, Time-frequency characteristics extraction of vehicle-track coupling system based on Hilbert-Huang transform, *Journal of vibration and shock*, vol. 32, no. 5, pp.43–47, 2013.
- [24] S. X. Chen, J. H. Lin, Influence of wheel ovalization on time-frequency characteristics of a high speed train based on improved HHT, *Journal of vibration and shock*, vol. 32, no. 11, pp. 126–130, 2013.
- [25] L. F. Weng, J. H. Lin, Track irregularity analysis based on wavelet transform, *China Measurement Technology*, vol. 31, no. 1, pp. 62–79, 2006.
- [26] H. C. Tsai, et al., Fast inspection and identification techniques for track irregularities based on HHT analysis, *Advances in Adaptive Data Analysis*, vol.4, pp.1250016-1-1250016-26, 2012.
- [27] H. C. Tsai, et al., Railway track inspection based on the vibration response to a scheduled train and the Hilbert-Huang transform, *Proc IMechE Part F:Journal Rail and Rapid Transit*, vol. 229, no. 7, pp.815–829, 2015.
- [28] X. J. Deng, et al., Influence of Corrugation on Time-frequency Characteristics of a Train Based on Improved Hilbert-Huang Transform, *Acta electronic Sinica*, vol. 44, no. 10, pp.2294-2299, 2016.
- [29] W. M. Zhai, Vehicle track coupling dynamics, *Science Press*, 2007.
- [30] N. E. Huang, et al., The empirical mode decomposition and the Hilbert spectrum for nonlinear and non-stationary time series analysis, *Proc. R. Soc. Lond. A*, 1998.
- [31] N. E. Huang, Computer Implemented Empirical Mode Decomposition Method, Apparatus, and Article of Manufacture, *USA, Provisional Application*, vol. 5, no. 983, 162, Nov.9, 1999.